Regulation of clathrin-mediated endocytosis by hierarchical allosteric activation of AP2

Zuzana Kadlecova,[1] Stephanie J. Spielman,[2] Dinah Loerke,[3] Aparna Mohanakrishnan,[1] Dana Kim Reed,[1] and Sandra L. Schmid[1]

[1]Department of Cell Biology, University of Texas Southwestern Medical Center, Dallas, TX 75390
[2]Institute for Genomics and Evolutionary Medicine, Temple University, Philadelphia, PA 19122
[3]Department of Physics and Astronomy, University of Denver, Denver, CO 80208

The critical initiation phase of clathrin-mediated endocytosis (CME) determines where and when endocytosis occurs. Heterotetrameric adaptor protein 2 (AP2) complexes, which initiate clathrin-coated pit (CCP) assembly, are activated by conformational changes in response to phosphatidylinositol-4,5-bisphosphate (PIP2) and cargo binding at multiple sites. However, the functional hierarchy of interactions and how these conformational changes relate to distinct steps in CCP formation in living cells remains unknown. We used quantitative live-cell analyses to measure discrete early stages of CME and show how sequential, allosterically regulated conformational changes activate AP2 to drive both nucleation and subsequent stabilization of nascent CCPs. Our data establish that cargoes containing Yxxφ motif, but not dileucine motif, play a critical role in the earliest stages of AP2 activation and CCP nucleation. Interestingly, these cargo and PIP2 interactions are not conserved in yeast. Thus, we speculate that AP2 has evolved as a key regulatory node to coordinate CCP formation and cargo sorting and ensure high spatial and temporal regulation of CME.

Introduction

Clathrin-mediated endocytosis (CME) is the major pathway by which receptors and their ligands are concentrated and taken up into cells (Conner and Schmid, 2003; McMahon and Boucrot, 2011). CME is fundamental to cell nutrition, neurotransmission, and cellular signaling. CME begins with an initiation step in which adaptors nucleate clathrin assembly, forming nascent clathrin-coated pits (CCPs; Owen et al., 2004; Cocucci et al., 2012; Traub and Bonifacino, 2013). CCPs recruit cargo, grow, and gain curvature through continued adaptor-dependent polymerization of clathrin (Godlee and Kaksonen, 2013; Kirchhausen et al., 2014). CCPs then undergo a maturation process involving multiple endocytic accessory proteins that results in formation of deeply invaginated CCPs (Schmid and McMahon, 2007; Merrifield and Kaksonen, 2014). Finally, the GTPase dynamin assembles into collar-like structures at the necks of CCPs, where it catalyzes membrane fission and vesicle release (Schmid and Frolov, 2011; Ferguson and De Camilli, 2012; Morlot and Roux, 2013).

Adaptor protein 2 (AP2), the major clathrin adaptor protein, is a heterotetramer (α, β2, μ2, and σ2 subunits) that forms a large globular core structure with two appendage domains connected via long flexible linkers (Collins et al., 2002; Jackson et al., 2010; Kirchhausen et al., 2014). The α and β2 subunits contribute the appendage domains, and interactions of the β2 appendage domain and linker with clathrin are required for clathrin assembly (Shih et al., 1995; Traub et al., 1999; Kelly et al., 2014). The appendage domain of the α subunit binds to and recruits endocytic accessory proteins during the maturation process (Owen et al., 1999; Praefcke et al., 2004). The core is composed of the N-terminal domains of α and β2 subunits, as well as the μ2 and σ2 subunits that, respectively, bind to either Yxxφ-based (where φ indicates a hydrophobic residue) or dileucine (diLeu)-based (Ohno et al., 1996; Owen and Evans, 1998; Kelly et al., 2008; Mattera et al., 2011) internalization motifs on transmembrane cargo proteins. AP2 also harbors three spatially distinct phosphatidylinositol-4,5-bisphosphate (PIP2) binding sites, one on each of the α, β2, and μ2 subunits (Gaidarov and Keen, 1999; Collins et al., 2002; Höning et al., 2005). A comparison of the crystal structures of the AP2 core, solved in the presence or absence of a bound cargo peptide, shows that AP2 undergoes a large conformational change from a "closed," cargo-inaccessible state to an "open" (i.e., active) conformation (Jackson et al., 2010). In the closed state, the clathrin binding site in the linker is buried within the core; hence AP2 is also unable to bind clathrin (Kelly et al., 2014).

In vitro biochemical studies have suggested that the transition from the closed to open state requires PIP2 binding, is

Correspondence to Sandra L. Schmid: sandra.schmid@utsouthwestern.edu

Abbreviations used: AAK1, adaptor-associated kinase 1; CCP, clathrin-coated pit; CLS, clathrin-labeled structure; CME, clathrin-mediated endocytosis; PIP2, phosphatidylinositol-4,5-bisphosphate; PM, plasma membrane; sCLS, subthreshold CLS; Tfn, transferrin; TfnR, Tfn receptor; TIRF, total internal reflection fluorescence; WT, wild-type.

The Rockefeller University Press $30.00
J. Cell Biol. Vol. 216 No. 1 167–179
https://doi.org/10.1083/jcb.201608071

further stabilized by binding cargo peptides (Höning et al., 2005; Jackson et al., 2010; Kelly et al., 2014), and may be favored by phosphorylation of the µ2 subunit by adaptor-associated kinase 1 (AAK1; Ricotta et al., 2002). Which of these multiple interactions is required in vivo, their functional hierarchy, and how the different conformational states relate to the dynamic sequence of early events in CME has not been explored.

In this work, we used sensitive live-cell total internal reflection fluorescence (TIRF) microscopy (Merrifield et al., 2002) in combination with biochemical measurements to dissect the role of low-affinity interactions with PIP2 or cargo as regulators of AP2 activation. We asked which of these interactions controls successful CCP nucleation and what is the functional and temporal relationship between the three distinct PIP2 and two cargo binding sites for CCP initiation and maturation. Finally, we investigated whether Yxxφ and diLeu cargo play identical roles in CCP initiation.

To address these outstanding questions in a cell-based system, we generated stable cell lines in which wild-type (WT) AP2 subunits are replaced with mutant subunits expressed at endogenous levels. These cell lines also stably overexpress CLCa-EGFP, which incorporates into clathrin triskelions without affecting the concentration of clathrin heavy chains or perturbing CME (Gaidarov et al., 1999; Ehrlich et al., 2004; Taylor et al., 2011; Aguet et al., 2013). This approach allows simultaneous, unbiased, live-cell visualization of thousands of CCPs at a time. The comprehensive nature of this analysis allows measurement of the rates of CCP nucleation, initiation, growth, and maturation (Mettlen and Danuser, 2014) and provides robust detection and tracking of even dim, nascent CCPs (Aguet et al., 2013). Most importantly, it allows measurements of the rate and extent of clathrin assembly at nascent CCPs (Loerke et al., 2011), which is a proxy for AP2 activity at the plasma membrane (Kelly et al., 2014).

Our results establish that the allosteric regulation of AP2 plays a critical role in vivo not only for directing nucleation, as was predicted, but also in subsequent stages to regulate the stepwise growth, stabilization, and maturation of nascent CCPs. This regulation involves the hierarchical interaction of multiple subunits with PIP2, as well as µ2 interactions with Yxxφ-containing cargo. We also found that AP2 interactions with cargoes containing Yxxφ motif, but not diLeu motif, critically regulate early stages of AP2 activation and CCP nucleation.

Results

To define the functional consequences and temporal hierarchy of AP2 activation by low-affinity interactions with PIP2 and cargo, we first established a library of htertRPE cell lines stably expressing siRNA-resistant AP2 mutants. These included hypomorphic mutations in α and β2 subunits defective in PIP2 binding, mutations in the µ2 subunit defective in PIP2 or Yxxφ-based cargo binding, and mutations in the σ2 subunit defective in binding diLeu-based cargo (Fig. 1, A and B). All mutations were designed based on known AP2 structures. Importantly, all mutants have been previously analyzed for correct folding, and their biochemical properties have been confirmed and characterized in vitro (Fig. 1 B; Owen and Evans, 1998; Collins et al., 2002; Höning et al., 2005; Kelly et al., 2008). The stable cell lines were selected by FACS to ensure that the levels of expression of mutant subunits were comparable to those of the endogenous subunits. To ensure full substitution, we also treated cells with siRNA to knock down endogenous subunits. Finally, we verified full incorporation of mutant subunits within AP2 complexes by immunoprecipitation of AP2α and immunoblotting for the mutated subunit (Fig. S1). Expression of mutant subunit and its localization in CCPs was also monitored by immunofluorescence (Fig. S1 F).

These mutations in individual subunits reduce, but do not completely eliminate, intact AP2 activity, which is required for CCP initiation (Motley et al., 2006; Aguet et al., 2013). Hence the temporal and functional hierarchy of these low-affinity interactions can be inferred through the quantitative analyses of CCP dynamics using live-cell TIRF microscopy (Fig. 1 C). We previously developed a highly sensitive object-based detection method to accurately detect all clathrin-labeled structures (CLSs) and quantitative methods to distinguish subthreshold CLSs (sCLSs) from bona fide CCPs (Aguet et al., 2013). sCLSs, which are short-lived and dim, include AP2-independent stochastic clathrin assemblies that occur within the TIRF field (i.e., <100 nm from the cell surface), as well as AP2-dependent early nucleation events that fail to grow (Fig. 1 C; Aguet et al., 2013). In contrast, bona fide CCPs are quantitatively defined by the continued accumulation of clathrin and growth past a threshold intensity (Fig. 1 C; see Materials and methods). In addition, a fraction (30–50%) of bona fide CCPs fail to mature and are aborted (Ehrlich et al., 2004; Loerke et al., 2009; Aguet et al., 2013). Abortive CCPs fail to gain curvature or recruit a burst of dynamin-2 before disappearing from the TIRF field. We quantified the effect of the AP2 mutations on sequential stages of CCV formation by measuring multiple independent properties of CCP dynamics, including the initiation density of sCLSs and bona fide CCPs, the rate and extent of clathrin assembly, and the efficiency of CCP maturation, as assessed by the fraction of short-lived (<20 s) abortive and longer-lived (40–60 s) productive CCPs (Fig. 1 C).

AP2α–PIP2 interactions are required at multiple early stages of CME

Previous studies have shown that bulk depletion of plasma membrane PIP2 abolishes CCP assembly (Boucrot et al., 2006; Zoncu et al., 2007). However, because many components of the endocytic and cytoskeletal machinery bind PIP2 and these experiments involved its prolonged depletion, the specific roles of AP2–PIP2 interactions in CCP nucleation and their potential roles after initiation remain unknown. Moreover, the functional and temporal hierarchy of the three spatially distinct PIP2 binding sites (Fig. 1 B) and their roles in AP2 activation in cells have not been defined. Therefore, we analyzed the effects of mutating each site independently. To validate our approach, verify the sensitivity of our live-cell imaging tools, and set a point of reference for other AP2 mutations, we first analyzed the role of the surface-accessible PIP2 binding site on the α subunit (Fig. 2 A). The consequence of abrogation of α–PIP2 interaction on clathrin assembly is relatively well understood in vitro (Kelly et al., 2014), and previous studies reported an ∼50% decrease in CME of transferrin (Tfn) in cells expressing this mutant (Motley et al., 2006), but the effects on CCP dynamics have not been studied.

In cells expressing α^{PIP2-}, the rates of initiation of bona fide CCPs were reduced by ∼60% (Fig. 2 B), providing a mechanism for the reported defect in CME. Importantly, we also observed an ∼50% decrease in the rate of appearance of

A

Perturbation	AP2 subunit	Mutant	Mutation
Ablate PIP2 binding	α	α^{PIP2-}	K57E/Y58E
	β2	$\beta2^{PIP2-}$	K5/12/26/27/29/36E
	μ2	$\mu2^{PIP2-}$	K341E/ K34E3/K345E
Ablate Tyr cargo binding	μ2	$\mu2^{cargo-}$	F174A/D176S
Ablate di-Leu cargo binding	σ2	$\sigma2^{cargo-}$	V88D

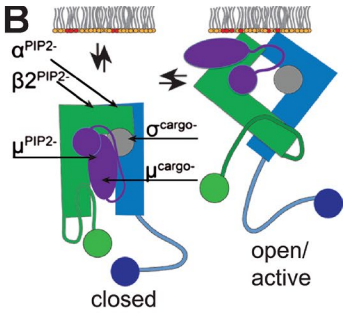

Figure 1. **AP2 mutants and TIRFM-based assays used in this study.** (A) Table listing the in vitro biochemical phenotypes of mutant AP2 subunits, their designations, and the residues mutated. (B) Schematic representation showing the positions of mutated residues with respect to the closed (left) and open (right) conformations of AP2. (C) Schematic representation of the CCP parameters measured by TIRF imaging and quantitative image analysis in this work. Tyr, tyrosine.

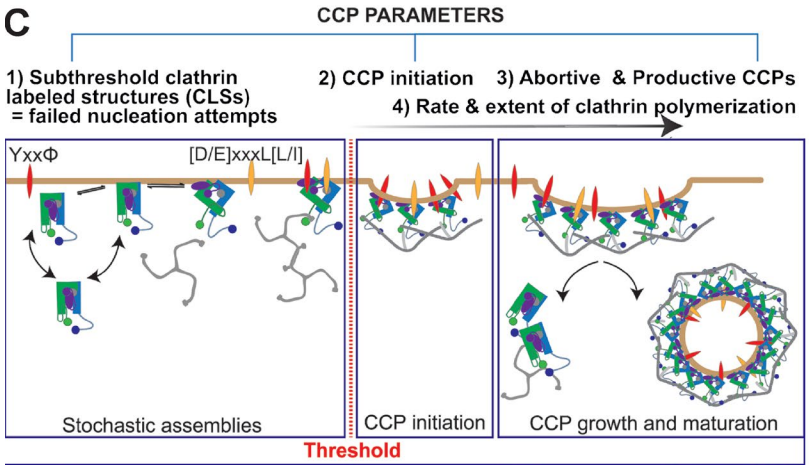

sCLSs, which represent failed nucleation attempts. Thus, the α–PIP2 binding site plays a critical role at the very earliest stages of CCP nucleation to ensure activation of AP2 only at the plasma membrane (PM).

To more directly assess AP2 activity, we measured the rates and extents of clathrin recruitment to nascent CCPs by measuring changes in CLC-EGFP intensity for bona fide CCPs binned within distinct lifetime cohorts. We observed a 30% decrease in the extent of clathrin assembly at CCPs in α^{PIP2-} mutant cells for all lifetime cohorts (Fig. 2 C). Because we confine our analyses to diffraction-limited CCPs (Aguet et al., 2013), these data indicate that even productive CCPs formed in the presence of this AP2 mutant were smaller. Importantly, the rate of clathrin polymerization, measured during the initial phase of CCP growth, (Fig. 2 D) also decreased by ∼45% in the α^{PIP2-} mutant cells compared with WT cells (Fig. 2 D and

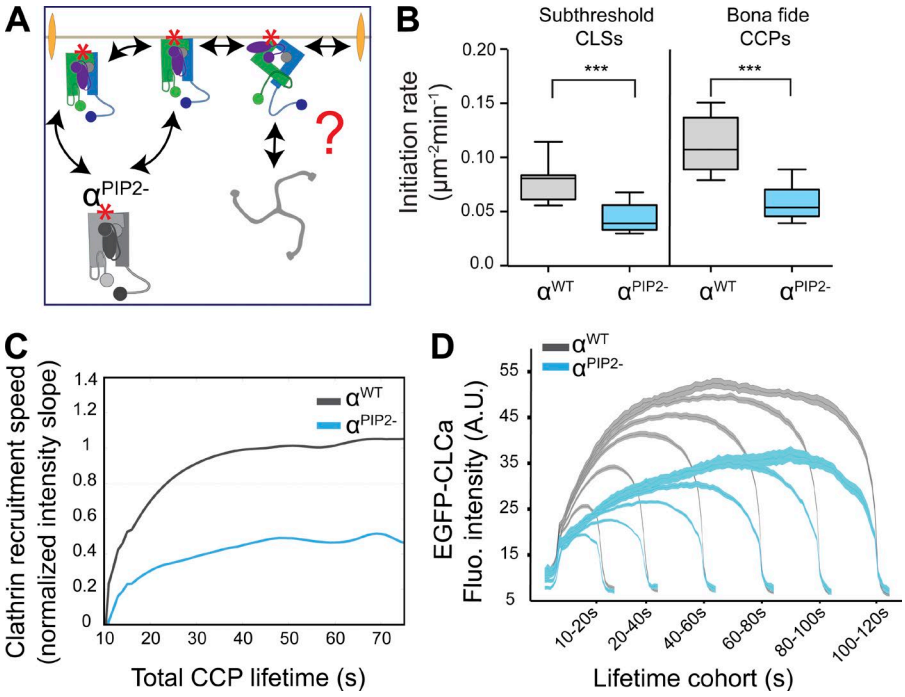

Figure 2. **Binding of PIP2 to the α subunit is essential for allosteric activation of AP2 to trigger clathrin polymerization and CCP initiation.** (A) Schematic representation of the possible early roles of α–PIP2 interactions. The question mark and double arrowheads point to potential roles in enhancing the rates and or extents of clathrin polymerization, CCP nucleation, cargo recruitment, and CCP maturation. (B) Initiation density of all detected subthreshold CLSs and bona fide CCPs for the indicated wt or mutant cells (≥15 cells per condition, #CCPs α^{wt} 32,320, #CCPs α^{PIP2-} 20,510). Box plots show medians, 25th and 75th percentiles, and outermost data points. ***, $P \leq 0.001$, unpaired *t* test. (C) Mean clathrin fluorescence intensity traces of lifetime cohorts of CCPs from α^{wt} (gray) and α^{PIP2-} (blue) cells. Intensities are shown as mean ± SE calculated from ≥15 cells per condition. (D) The slope of intensity trace (averaged in the time interval 3–8 s of the elapsed lifetime) in α^{wt} and α^{PIP2-} cells. A.U., arbitrary units; Fluo., fluorescence.

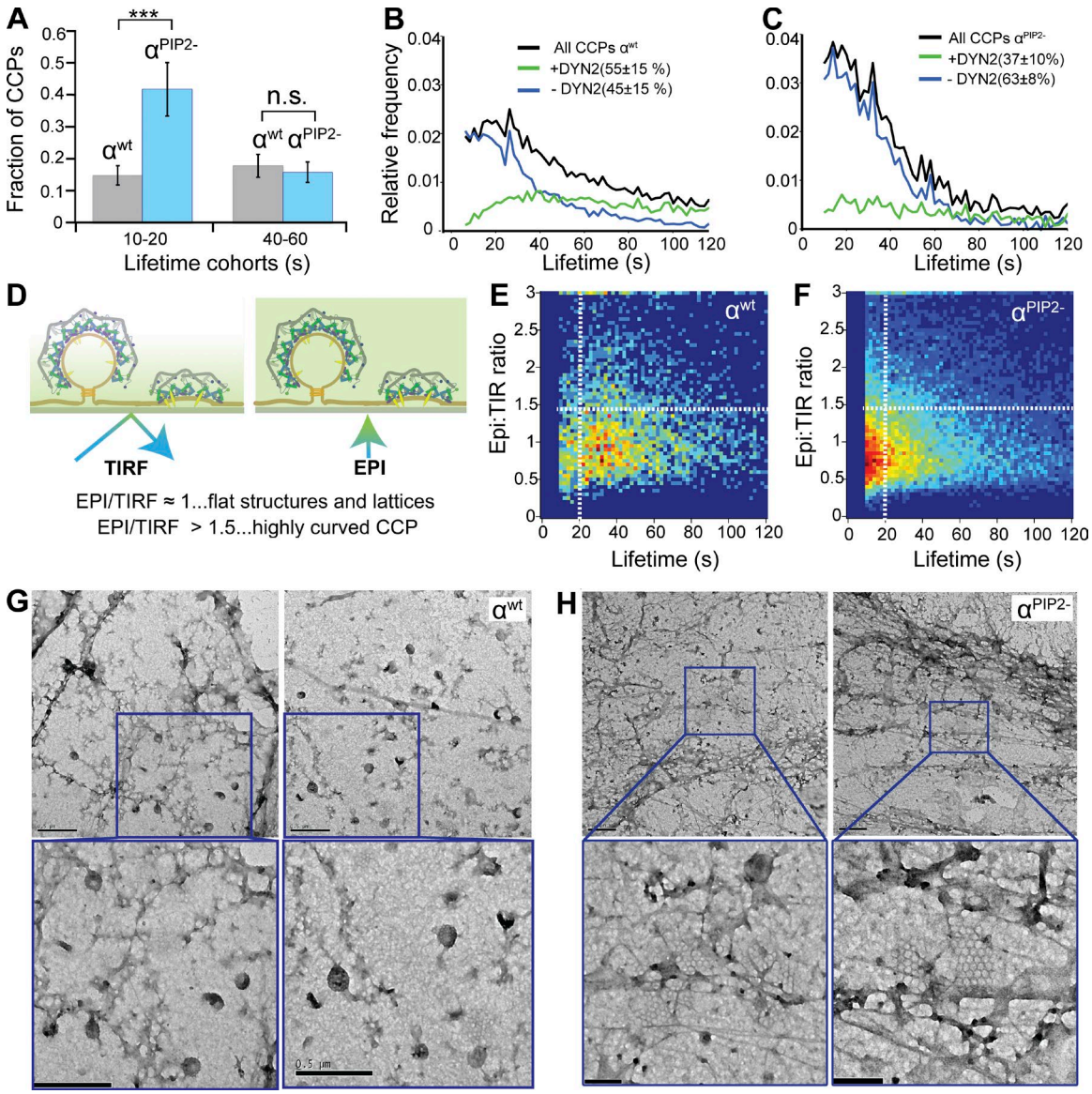

Figure 3. **Sustained binding of PIP2 to AP2 α subunit is required for CCP maturation.** (A) Fraction of CCPs found in short-lived versus longer-lived lifetime cohorts in α^{WT} (gray) and α^{PIP2-} (blue) cells. Data shown are mean ± SD (n > 100,000 CCPs from three independent experiments); n.s., not significant; ***, $P < 0.001$. Lifetime distributions of all bona fide CCPs (black lines), dynamin-2 (DYN2)-positive CCPs (green lines), and DYN2-negative CCPs (blue lines) in α^{WT} (B) and α^{PIP2-} (C) cells. (D) The ratio of epifluorescence (EPI):TIRF intensity levels for individual CCPs is indicative of curvature acquisition. EPI:TIRF ratio for individual CCPs plotted as a function of CCP lifetime in α^{WT} (E) and α^{PIP2-} (F) cells. Heatmap indicates frequency. EM images of "unroofed" hTertRPE cells reconstituted with either α^{WT} (G) or α^{PIP2-} (H). Bottom panels show higher-magnification view of the indicated area. Bars: (top) 500 nm; (bottom) 200 nm.

Fig. S2). These results establish that α–PIP2 interactions are required to regulate clathrin polymerization at nascent CCPs. The initial rate of clathrin recruitment is critical for stabilizing nascent CCPs, as shorter-lived CCPs recruited clathrin at slower initial rates than longer-lived CCPs (Figs. 2 D and S2). This was true in both WT and mutant cells (Fig. 2 C).

Whether AP2–PIP2 interactions are required for subsequent stages of CCP maturation remains an open question. Indeed, it has been suggested based on theoretical considerations (Schmid and McMahon, 2007) and in vitro studies (Dannhauser and Ungewickell, 2012) that clathrin assembly is sufficient to drive subsequent stages of CME. To test this, we next analyzed the role of α–PIP2 interactions on the lifetime distribution of bona fide CCPs, a measure of CCP maturation. α^{PIP2-} cells exhibited a significant increase in the fraction of shorter-lived (≤20 s) CCPs compared with WT cells (Fig. 3 A); whereas longer-lived (40–60 s) populations were unaffected. These data suggest a defect in CCP maturation and an increase in abortive events. Consistent with this interpretation, we also observed a decrease in the fraction of CCPs that recruit dynamin-2 (from 55% in WT cells to ∼37% in α^{PIP2-} cells; Fig. 3 C; Taylor et al., 2012; Aguet et al., 2013; Grassart et al., 2014). These results establish that α–PIP2 interactions are required beyond initiation to stabilize nascent CCPs.

To further characterize the defect in CCP maturation, we analyzed CCP dynamics using near-simultaneous TIRF and epifluorescence microscopy. In TIRF, the evanescent illumination field decays exponentially as it penetrates the adherent cell surface; therefore, the ratio between TIRF and epifluorescence intensities provides a measure of CCP curvature acquisition as

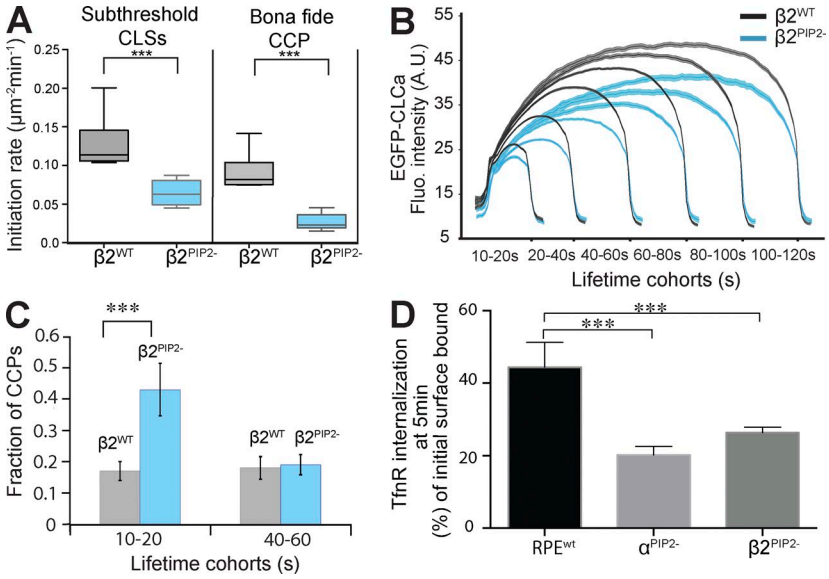

Figure 4. **Binding of PIP2 to AP2 β subunit is equally essential for efficient CCP initiation and clathrin polymerization.** (A) Initiation density of subthreshold CLSs and bona fide CCPs for the indicated wt or mutant cells (18 cells per condition). Box plots show medians, 25th and 75th percentiles, and outermost data points. ***, $P \leq 0.001$, unpaired *t* test. (B) Mean clathrin fluorescence intensity traces in lifetime cohorts of CCPs from $\beta2^{wt}$ (gray) and $\beta2^{PIP2-}$ (blue) reconstituted cells. Intensities are shown as mean ± SE calculated from 18 cells per condition. A.U., arbitrary units; Fluo., fluorescence. (C) Fraction of CCPs found in short-lived versus longer-lived cohorts for β^{WT} (gray) and β^{PIP2-} (blue) cells. ***, $P < 0.001$. (D) Transferrin receptor internalization was measured in β^{WT}, α^{PIP2-}, and β^{PIP2-} cells using a monoclonal anti-TfnR antibody as ligand. Percentage of TfnR uptake was calculated relative to the initial total of surface-bound antibody. Data represent mean ± SD, $n = 4$. ***, $P \leq 0.005$, unpaired *t* test.

a function of lifetime (Saffarian and Kirchhausen, 2008; Aguet et al., 2013; Fig. 3 D). We detected a twofold increase in the number of flat structures (TIRF/epifluorescence ≤1) with short lifetimes (≤20 s) in α^{PIP2-} cells (Fig. 3 F) compared with WT cells (Fig. 3 E). These small, flat CCPs could be directly observed by negative-stain electron microscopy in α^{PIP2-} cells (Fig. 3, G and H). Additionally, abrogation of α–PIP2 binding led to a decreased concentration of both cargo and AP2 at CCPs (Fig. S3). Together, these effects lead to an increase in the number of abortive events.

Altogether, our data explain the observed defect in CME in α^{PIP2-} cells (Motley et al., 2006). We show that CCP nucleation in cells is dependent on activation of AP2 through interactions between plasma membrane PIP2 and the surface exposed binding site on the α-subunit. Moreover, these interactions play a critical role not just in nucleating clathrin assembly at nascent CCPs, but in all subsequent steps of CME, including CCP stabilization, growth, maturation, and cargo recruitment.

AP2 β2–PIP2 interactions are equally critical for early stages of CME

The β2-subunit of AP2 encodes a second PIP2 binding site, formed by six surface-exposed lysine residues (Collins et al., 2002; Jackson et al., 2010), which has not been studied in vivo. We find that $\beta2^{PIP2-}$ cells (Fig. 1 and Fig. S1, B and F). phenocopied α^{PIP2-} cells in that they exhibited decreased rates of initiation of both sCLSs and bona fide CCPs (Fig. 4 A), reduced extents of clathrin polymerization at bona fide CCPs (Fig. 4 B), and a shift in lifetime distribution toward short-lived versus productive CCPs (Fig. 4 C). Consistent with these findings, CME of transferrin receptors was inhibited by ∼50% in $\beta2^{PIP2-}$ cells, the same extent seen in α^{PIP2-} cells (Fig. 4 D). Thus, we conclude that although the α– and β2–PIP2 binding sites can operate independently, full allosteric activation of AP2, which is needed in cells to trigger rapid clathrin assembly and efficient CCP maturation, requires binding of PIP2 to both α and β2 subunits.

μ2–PIP2 binding provides downstream stabilization of AP2 at the PM

The μ2 subunit is pivotal for AP2 function. It harbors a third PIP2 binding site (Collins et al., 2002; Jackson et al., 2010; Fig. 5 A) and is essential for Yxxφ-based cargo recognition (Ohno et al., 1995; Owen and Evans, 1998). It is also a substrate for phosphorylation by AAK1 (Olusanya et al., 2001; Conner and Schmid, 2002; Ricotta et al., 2002). The PIP2 binding site on μ2 is located at the C terminus and is in the closed conformation (Figs. 1 B and 5 A; Jackson et al., 2010). There are contradictory findings as to whether μ2–PIP2 interactions are required for CME. One study reported a strong dominant negative effect of overexpression of a μ2 mutant defective in PIP2 binding (Rohde et al., 2002), whereas a second study showed that the same μ2 mutant could fully rescue CME in μ2-deficient cells (Motley et al., 2006). We reproduced the latter finding by showing that Tfn uptake was unaffected in htertRPE cells reconstituted with the identical $\mu2^{PIP2-}$ mutant (Fig. S4 A).

We next applied our more sensitive live-cell imaging assays to more directly test whether the PIP2 binding site on μ2 plays a role in AP2 activation and early stages of CME. Unexpectedly, and in diametric contrast to results obtained when surface-localized PIP2 binding sites were disrupted, we observed an increased rate of initiation of bona fide CCPs (Fig. 5 B) and an increased rate and extent of clathrin recruitment to CCPs in the $\mu2^{PIP2-}$ cells (Fig. 5, C and D). No significant changes in the rates of appearance of stochastic assemblies or early nucleation events (i.e., sCLSs) were observed, indicating that μ2–PIP2 binding is not required for these earliest steps.

Importantly, the increased rate of CCP initiation and growth of CCPs in $\mu2^{PIP2-}$ cells was not associated with a higher likelihood of vesicle formation. Thus, as observed with the α^{PIP2-} and $\beta2^{PIP2-}$ mutants, there was a significant increase in the fraction of short-lived, presumably abortive CCPs in the $\mu2^{PIP2-}$ cells compared with $\mu2^{WT}$ cells (Fig. 5 E). Correspondingly, we observed an increase in short-lived, flat CCPs (Fig. S4, B and C) and a decrease in the fraction of dynamin-2–positive CCPs (from 55% to 42%; Fig. 5 F). Unlike in $\alpha/\beta2^{PIP2-}$ mutants, the recruitment of cargo into CCPs and the quantity of AP2 in $\mu2^{PIP2-}$ CCPs was not affected (Fig. S3). Finally, given that the PIP2 binding site on μ2 corresponds to two large patches (Jackson et al., 2010) we also examined the effect of mutating additional positively charged residues implicated in PIP2 binding (K167, R169, R170, K365, and K367) and obtained results similar to those described for $\mu2^{PIP2-}$ (unpublished data). From these

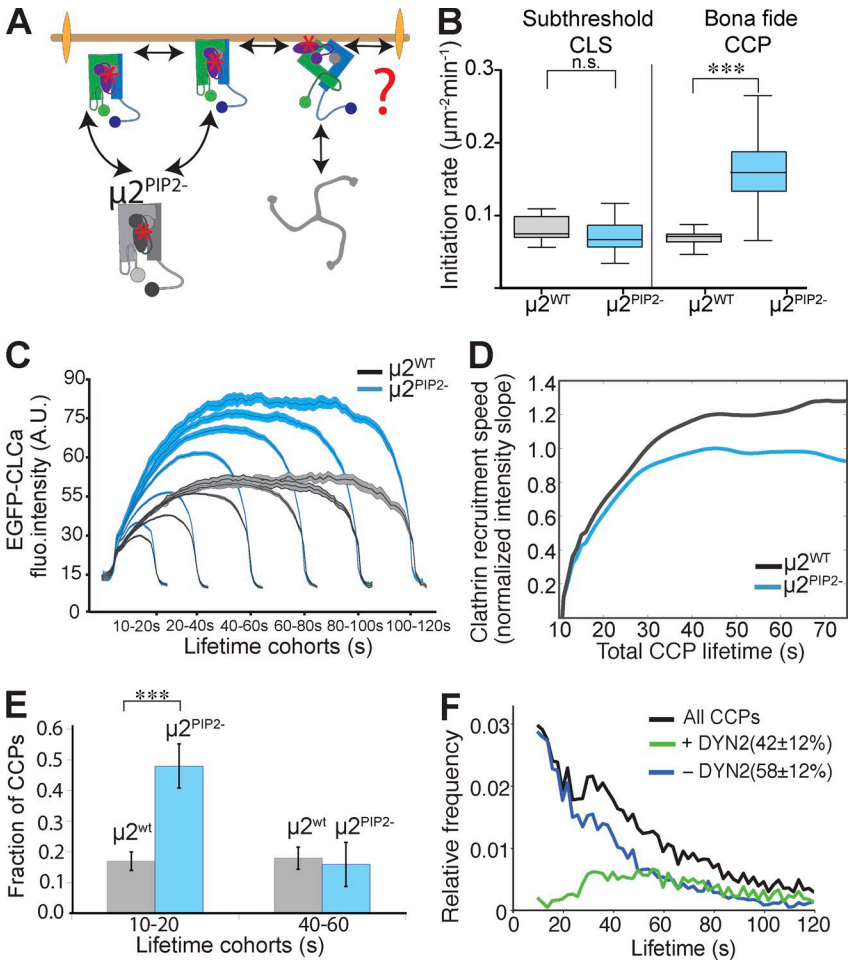

Figure 5. **Binding of PIP2 to the μ2 subunit is required downstream of initial AP2 activation for later stages of CCP maturation.** (A) Schematic representation of the possible early roles of α–PIP2 interactions. The question mark and double arrowheads point to potential roles in enhancing the rates and or extents of clathrin polymerization, CCP nucleation, cargo recruitment, and CCP maturation. (B) Initiation density of all subthreshold CLSs and bona fide CCPs for the indicated wt or mutant cells (≥22 cells per condition, #CCPs $\mu2^{wt}$ 27,943, #CCPs $\mu2^{PIP2-}$ 36,523). Box plots show medians, 25th and 75th percentiles, and outermost data points. ***, $P \leq 0.0005$, unpaired *t* test. n.s., not significant. (C) Mean clathrin fluorescence intensity traces in lifetime cohorts of CCPs from $\mu2^{wt}$ (gray) and $\mu2^{PIP2-}$ (blue) reconstituted cells. Intensities are shown as mean ± SE calculated from 17 cells per condition. (D) Slope of intensity trace (averaged in the time interval 3–8 s of the elapsed lifetime) in $\mu2^{wt}$ (gray) and $\mu2^{PIP2-}$ (blue) cells. (E) Fraction of CCPs found in short-lived versus longer-lived lifetime cohorts in $\mu2^{WT}$ (gray) and $\mu2^{PIP2-}$ (blue) cells. ***, $P < 0.001$. (F) Lifetime distributions of all bona fide CCPs (black lines), dynamin-2 (DYN2)-positive CCPs (green lines), and Dyn2-negative CCPs (blue lines) in $\mu2^{PIP2-}$ cells.

studies, we conclude that μ2–PIP2 binding functions downstream of α– and β2–PIP2 interactions and is required for sustained activation of AP2 and efficient CCP maturation.

Increased AAK1 activity compensates for μ2-PIP2 binding deficiency

The increased rate of CCP initiation observed in $\mu2^{PIP2-}$ cells may reflect activation of a compensatory mechanism in response to the decreased efficiency of CCP maturation to restore CME to normal levels. Indeed, we have previously identified compensatory mechanisms that restored CME in cells expressing an α-appendage domain deletion mutant of AP2 (ΔαAD cells; Aguet et al., 2013). Tfn uptake was unaffected in the ΔαAD cells despite profound defects in CCP maturation (Aguet et al., 2013; Reis et al., 2015). We therefore tested whether alternate, compensatory mechanisms might also have restored efficient clathrin recruitment and CME in $\mu2^{PIP2-}$ cells.

The phosphorylation of μ2 on T156 by AAK1 has been proposed to stabilize the open conformation of AP2 (Ricotta et al., 2002; Jackson et al., 2010). Moreover, both in vitro (Conner et al., 2003) and in vivo (Jackson et al., 2003) evidence suggests that AAK1 activity is stimulated by assembled clathrin. Thus, we wondered whether the increase in the rate and extent of clathrin assembly in $\mu2^{PIP2-}$ cells might reflect the activation of an AAK1-dependent feed-forward loop (Fig. 6 A). To test whether increased AAK1 activity might be compensating for defects in CCP maturation in $\mu2^{PIP2-}$ cells, we measured levels of phosphorylation of T156 on μ2. $\mu2^{PIP2-}$ cells exhibited a 30% increase in T156 phosphorylation compared with $\mu2^{WT}$ cells (Fig. S4 D; quantified in Fig. 6 B). In contrast, μ2 T156 phosphorylation levels were reduced in α^{PIP2-} cells. To determine whether enhanced AAK1 activity was required to compensate for the PIP2 binding defect in μ2, we compared Tfn receptor (TfnR) internalization in control, $\mu2^{PIP2-}$, and α^{PIP2-} cells with and without treatment with a specific chemical inhibitor of AAK1 (Compound 2; Bamborough et al., 2008). Control experiments verified that Compound 2 effectively reduced μ2 phosphorylation (Fig. S4 E). As we predicted, TfnR uptake in $\mu2^{PIP2-}$ cells was much more sensitive to AAK1 inhibition than that in WT cells (~50% inhibition in $\mu2^{PIP2-}$ cells compared with ~20% in WT cells; Fig. 6 C). In contrast, the residual levels of TfnR internalization in α^{PIP2-} cells were unaffected by Compound 2, indicating that AAK1 is not active in these cells. Because AAK1 is recruited to CCPs through interactions with both AP2 and clathrin, this finding likely reflects the impaired rates of CCP initiation and growth in these mutant cells. We were unable to study the consequence of total ablation of μ2T156 phosphorylation because we found that the $\mu2^{T156A}$ mutant was poorly expressed and inefficiently incorporated into AP2 complexes (Fig. S1 E).

These results suggest that μ2–PIP2 binding promotes CCP maturation but that defects in this activity can be compensated for by activation of AAK1 and phosphorylation of μ2. Our results provide in vivo evidence that AAK1 phosphorylation can indeed drive a conformational change similar to that triggered by PIP2 and/or cargo binding to release clathrin binding sites

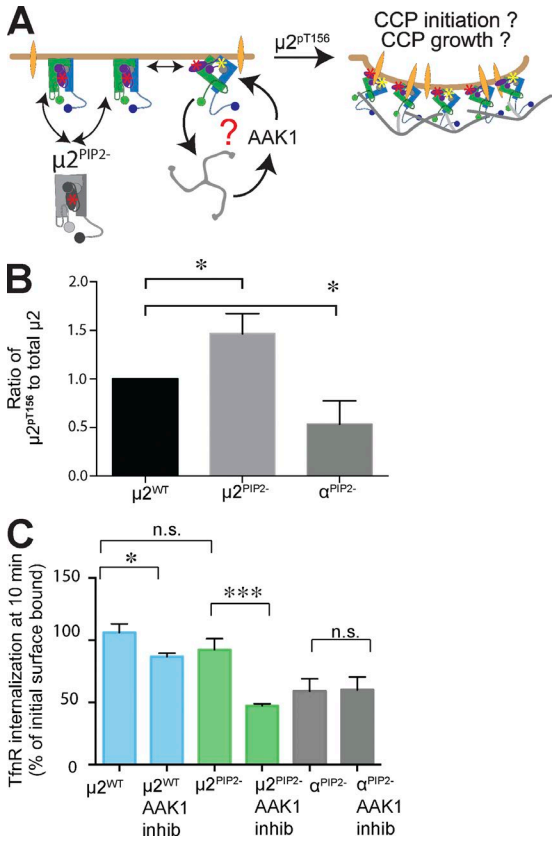

Figure 6. **Increased phosphorylation of μ2 at T156 compensates to maintain efficient TfnR internalization in μ2^{PIP2-} cells.** (A) Schematic representation of the potential roles for AAK1 activation and phosphorylation of T156 on μ2. The question mark and arrows point to possible compensatory mechanisms and a positive feed-forward loop that can restore efficient CME in μ2^{PIP2-} cells. (B) Quantification (mean ± SD, *n* = 3; two-tailed Student's *t* tests were used to assess statistical significance: *, P < 0.05) of total and phosphorylated μ2^{pT156} subunit in μ2^{WT}, μ2^{PIP2-}, and α^{PIP2-} cells (see also Fig. S5 B). (C) TfnR uptake measured at 10 min in control, μ2^{PIP2-}, and α^{PIP2-} cells with or without treatment with the 10-μM AAK1 inhibitor (inhib), Compound 2. Data shown are mean ± SD, *n* = 3; normalized to total surface bound; *, P < 0.05; ***, P < 0.0005. n.s., not significant.

and activate AP2 for clathrin assembly. Our data are also consistent with previous studies (Conner et al., 2003; Jackson et al., 2003) showing that clathrin assembly, which is enhanced in μ2^{PIP2-} cells but decreased in α^{PIP2-} cells, stimulates AAK1 activity. Together, these findings provide strong evidence for the role of AAK1-mediated phosphorylation of μ2 in providing positive feedback to enhance the clathrin assembly activity of AP2 (Fig. 6 A). We conclude that μ2–PIP2 binding operates in cells downstream of α– and β2–PIP2 interactions to stabilize active AP2 complexes already on the PM, thus enhancing the efficiency of growth and stabilization of bona fide CCPs. Importantly, our data show that sustained interactions of PIP2 with binding sites on all three subunits are required to maintain AP2 activation to ensure efficient CCP maturation and CME.

Essential role for cargo binding in CCP nucleation

Although a consensus is emerging that cargo recruitment can stabilize growing CCPs (Ehrlich et al., 2004; Loerke et al., 2009; Traub, 2009), whether AP2–cargo interactions are required for CCP nucleation remains a matter of debate (Godlee and Kaksonen, 2013). One group reported that AP2 and clathrin assembled several seconds before detection of cargo (Cocucci et al., 2012), and another group reported that TfnR are recruited concomitantly with AP2 and clathrin in nascent CCPs (Liu et al., 2010). Other studies approached this question by manipulating the levels, activities, or clustering of single cargo receptors (Loerke et al., 2009; Liu et al., 2010; Mettlen et al., 2010). We decided to take a different approach by globally eliminating the binding of one of the two major classes of internalization motifs, the Yxxφ motif and the diLeu motif, to AP2 (Fig. 7 A). Thus, we replaced endogenous subunits with either a μ2^{cargo-} mutant that is unable to bind cognate cargoes carrying the Yxxφ motif or a σ2^{cargo-} mutant that is unable to bind cargoes carrying the diLeu motif (Fig. 1 A). We first confirmed these phenotypes biochemically. As expected, internalization of a model Yxxφ cargo (CD8-YAAL; Fig. S5) was strongly impaired in the μ2^{cargo-} mutant cell line (>60% inhibition), whereas internalization of a model diLeu cargo (CD8-EAAALL; Fig. S5) was strongly impaired (>50% inhibition) in cells expressing σ2^{cargo-} (Fig. 7 B). Interestingly, whereas the uptake of the orthogonal, Yxxφ-based cargo was not significantly affected in the σ2^{cargo-} cells, diLeu cargo uptake was reduced in the μ2^{cargo-} cell line, albeit to a lesser extent (~30% inhibition) than either the cognate Yxxφ-containing (Fig. 7 B) or diLeu-containing cargo in the σ2^{cargo-} cells. These relative cargo-sorting activities were confirmed by directly measuring the concentration of different cargo molecules in CCPs (Fig. 7 C). σ2^{cargo-} cells were specifically defective in recruitment of diLeu cargo to CCPs, whereas μ2^{cargo-} cells showed a general defect in all cargo classes, including FXNPXY-containing cargo and the EGF receptor.

To explore the basis for the more general defect in CME caused by the μ2^{cargo-} mutant, we next looked at CCP dynamics. Cells expressing the μ2^{cargo-} mutant showed a significant decrease in initiation rates of both sCLSs and CCPs, whereas there was no effect in σ2^{cargo-} cells (Fig. 7 D). Similarly to α^{PIP2-} cells, we detected a decrease in the rate and extent of clathrin recruitment in all lifetime cohorts of bona fide CCPs (Fig. 7, E and F). Thus the μ2^{cargo-} mutant phenocopies the α^{PIP2-} and β^{PIP2-} mutants with regard to its effects on CCP initiation (Fig. 7 F). From this, we conclude that AP2–cargo interactions play an essential, early role in the activation of AP2 and productive nucleation of CCPs.

Our studies also reveal an apparent functional hierarchy in cargo binding, because interactions with Yxxφ-containing cargo showed a stronger and more global effect on CME than those of diLeu-containing cargo. This hierarchy could reflect the reported approximately threefold difference in binding affinity of AP2 to Yxxφ- versus diLeu-containing cargo motifs (Höning et al., 2005; Jackson et al., 2010) or differences in the ability of these two motifs to stabilize the open conformation of AP2 during early, critical stages of CCP assembly. If the former, then we would predict that overexpressing diLeu motif–containing cargo should, by mass action, rescue the μ2^{cargo-} defect in CCP initiation. However, adenoviral-driven overexpression of the diLeu-containing CD8 chimera failed to rescue the μ2^{cargo-} defect (Fig. 8 A), indicating that there is indeed a functional hierarchy of cargo binding sites in the core of the AP2 complex, and that the binding of Yxxφ-based cargo to μ2 plays a pivotal role in AP2 activation and CCP nucleation.

To further probe this potential functional hierarchy, we performed a bioinformatics analysis of the PM transmembrane-proteome based on identified internalization-coding

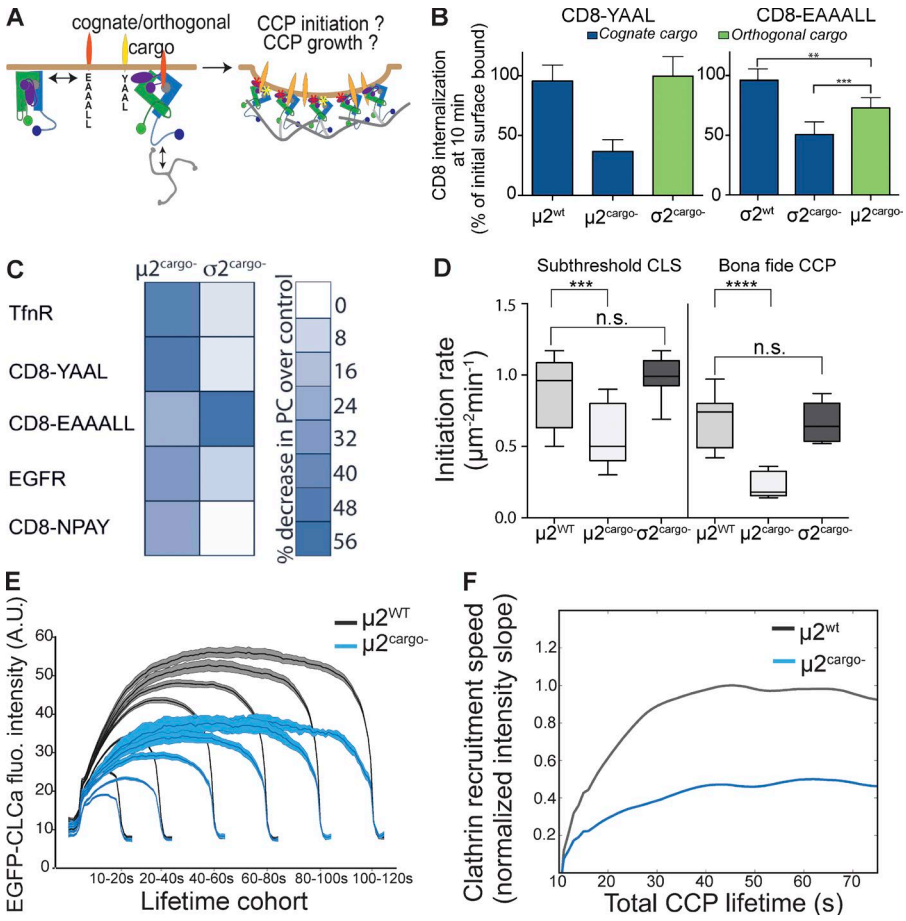

Figure 7. **Activation of AP2 by binding to YXXφ sorting signals is necessary for CCP nucleation.** (A) Schematic representation of the potential role of σ2 and μ2 interactions with their cognate (diLeu and YXXφ, respectively) or orthogonal cargo on AP2 activation and CCP nucleation. (B) Internalization of CD8 chimeras containing either the YXXφ (cognate for μ2, orthogonal for σ2) or diLeu (cognate for σ2, orthogonal for μ2) sorting signals was followed using CD8 mAb (data shown are mean ± SD, n = 3; normalized to total surface bound; **, P < 0.05; ***, P < 0.005). (C) Heatmap representing the changes in Pearson correlation coefficient (PC) between EGFP-CLCa, respective CD8 chimeras, and other CME cargo showing efficiency of cargo loading into CCPs in $\mu2^{cargo-}$ and $\sigma2^{cargo-}$ cells. (D) Initiation density of all detected CLSs and bona fide CCPs for the indicated wt or mutant cells (≥35 cells per condition, #CCPs $\mu2^{wt}$ 45,054, #CCPs $\mu2^{cargo-}$ 38,120). Box plots show medians, 25th and 75th percentiles, and outermost data points. ***, P < 0.0005; ****, P < 0.0001, t test. n.s., not significant. (E) Mean clathrin fluorescence (fluo.) intensity traces in lifetime cohorts of CCPs from $\mu2^{WT}$ (gray) and $\mu2^{cargo-}$ (blue) reconstituted cells. Intensities are shown as mean ± SE calculated from 20 cells per condition. A.U., arbitrary units. (F) Slope of intensity trace (averaged in the time interval 3–8 s of the elapsed lifetime) in $\mu2^{wt}$ (gray) and $\mu2^{cargo-}$ (blue) cells.

motifs, Yxxφ and diLeu. To account for the higher complexity of the diLeu motif, we included all previously reported variations (see Materials and Methods). Our analysis revealed that the internalization motifs are not equally distributed (Fig. 8 B): of 3,705 plasma membrane receptors, 1,250 (33%) uniquely contain a Yxxφ motif, whereas only 275 (7%) uniquely contain a diLeu motif. These results are consistent with our finding that Yxxφ motif–containing cargo function synergistically with PIP2 in vivo to efficiently nucleate CCPs and initiation cargo sorting and CME.

Discussion

AP2, which is absolutely required for CCP initiation in higher eukaryotes, is the most abundant endocytic adaptor, with an exceptionally high degree of conservation of all subunits from yeast to human (Schledzewski et al., 1999). Initiation of productive CCPs requires nucleation, rapid growth, and stabilization. Quantitative analysis in living cells allowed us to measure these discrete early stages of CME and revealed how sequential allosterically regulated conformational changes in AP2 adaptors are required to drive the vectorial nature of these events. We show that interactions with both PIP2 and cargo are required for full activation of AP2 to couple cargo detection and sorting with efficient CCP formation and maturation. Our data establish the following sequence: (1) AP2 activation via α– and β2–PIP2 binding and Yxxφ cargo recruitment drives clathrin polymerization at the PM and CCP nucleation; (2) stabilization of active AP2 complexes on the PM occurs via μ2–PIP2 engagement or μ2-T156 phosphorylation, which itself is regulated via assembled clathrin through an AAK1-dependent feedback loop to enhance clathrin polymerization; and (3) sustained interactions of PIP2 with binding sites on α, β2, and μ2 are required for CCP stabilization and efficient maturation (Fig. 8 C). Thus, in contrast to previous suggestions that clathrin interactions substitute for early AP2 interactions in stabilizing nascent CCPs and driving CCP maturation (Schmid and McMahon, 2007), our results establish a sustained requirement for active AP2 complexes.

Recent studies have proposed that the muniscin family of endocytic accessory proteins (FCho and SGIP) can activate AP2 in cells (Hollopeter et al., 2014; Umasankar et al., 2014), and while this study was in preparation, a new article (Ma et al., 2016) suggested that AP2 recruitment to sites of CCP formation is assisted by preformed FCHO-Eps15 complexes. In that model, the capture of AP2 reflects the formation of FCho–Eps15–AP2 nanoclusters, and AP2–PIP2 interactions are required only subsequently. Although the formation of nanoclusters may lead to an increase in AP2 residence time on the PM, our data show that in the presence of endogenous levels of FCho and Eps15, efficient AP2 recruitment to the PM and CME initiation is entirely dependent on the AP2–PIP2 and AP2–cargo interactions. Consistent with this, redirection of the FCho μ homology domain to the Golgi is sufficient to recruit Eps15, but not AP2, complexes (Ma et al., 2016), presumably because of the lack of PIP2 on Golgi membranes.

Altogether, our findings reveal that a temporal hierarchy of interactions govern AP2 activation to regulate early stages of

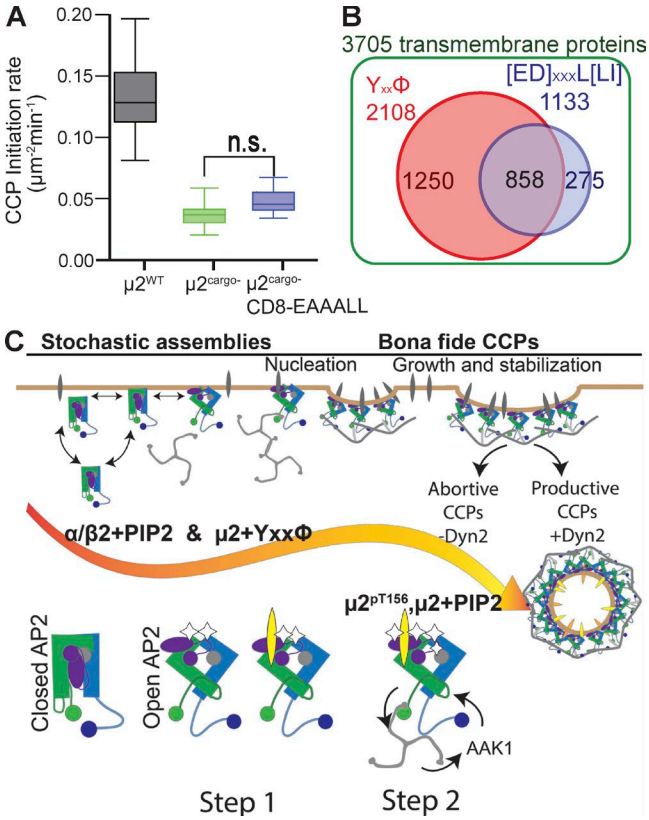

Figure 8. **Selective role of YXXφ-bearing cargo for AP2 activation and model for sequential allosteric regulation of AP2 by PIP2 and cargo interactions.** (A) Overexpression of CD8 chimera containing a diLeu sorting motif does not rescue initiation of CCPs in μ2^{cargo-} cells (≥16 cells per condition; CCPs μ2^{wt} 18,235, #CCPs μ2^{cargo-} 16,573, #CCPs μ2^{cargo-}[CD8-EAA ALL] 15,836). n.s., not significant. (B) Bioinformatics search for human transmembrane proteins containing YXXφ- or diLeu-based sorting motif revealed overrepresentation of YXXφ motif–bearing cargo. (C) Model for regulation of CCP nucleation and maturation through allosteric activation of AP2 by sequential and hierarchical interactions with its ligands, PIP2, and YXXφ-bearing cargo. Initiation (step 1) involves interactions between surface-exposed PIP2-binding sites on both the α and β2 subunits, as well as interactions between YXXφ-bearing cargo and the μ2 subunit to allow AP2 to recruit clathrin. Rapidly assembling clathrin (step 2) can activate AAK1 kinase, which phosphorylates μ2, creating a positive feed-forward loop that drives efficient CCP maturation. Full activation of AP2, which is required for CCP growth and stabilization, occurs when the μ2 subunit also engages PIP2. Early CCP intermediates formed by AP2 mutants defective in α–, β2–, or μ2–PIP2 binding are impaired in curvature generation and the recruitment of dynamin-2 (Dyn2) and exhibit a greater tendency to abort.

CCP formation and stabilization. They also provide a molecular explanation for the contributions of both PIP2 (Antonescu et al., 2011) and cargo (Ehrlich et al., 2004; Loerke et al., 2009) to CCP maturation. Like AP2, most of the components of the CME machinery interact via low-affinity binding to divergent motifs that are broadly expressed on multiple components (Owen et al., 1999; Praefcke et al., 2004; Schmid and McMahon, 2007). Therefore, understanding the functional hierarchy of AP2 interactions with molecular precision has broad relevance, as it represents a general paradigm for cargo transport and sorting events (Pandey, 2009; Perkins et al., 2010; Van Roey et al., 2012).

Previous studies have shown that acute and bulk depletion of PIP2 from the PM results in loss of all CCPs (Boucrot et al., 2006; Zoncu et al., 2007). Our dissection of the specific roles of the three AP2–PIP2 binding sites reveals a previously unappreciated complexity and multiple roles for PIP2 throughout the lifetime of CCPs. Thus, we found that nucleation of all detectable clathrin assemblies was reduced by ∼50% when either of the surface-exposed PIP2 binding sites on α or β2 was mutated. Because previous studies showed that the rate of initiation of bona fide CCPs was nearly ablated upon siRNA knockdown of AP2 (Aguet et al., 2013), we interpret the difference to reflect the residual (∼50%) activity of a single surface PIP2 binding site on AP2. These data refine structural models (Kelly et al., 2014) and show that both α– and β2–PIP2 interactions are equally important for full activation of AP2 to expel the β2 clathrin binding site from the AP2 core and restrict clathrin assembly to the plasma membrane (Fig. 8 C).

Although in vitro studies have established a role for AAK1 in phosphorylating μ2 and stabilizing the open conformation of AP2, in vivo evidence of a role for AAK1 in CME is lacking (Pelkmans et al., 2005). Our finding that AAK1 activation can compensate for defects in μ2–PIP2 interactions suggests that AAK1 activity can be fine-tuned in response to defects in early stages of CME, in part through a positive feedback loop dependent on clathrin assembly (Fig. 8 C, step 2).

The role of cargo in CCP nucleation has been debated. Our data show that μ2 interactions with Yxxφ motif–containing cargo efficiently modulate AP2 activation at the PM and are required for CCP nucleation. In contrast, interactions between σ2 and diLeu-based cargo have little effect. This hierarchy in AP2–cargo binding in vivo is determined by (a) Yxxφ-containing cargo abundance and (b) their allosteric effect on AP2 activity. The differential allosteric effect of the two sorting signals on AP2 observed in our experiments could be explained by the different structural requirements for exposing the Yxxφ and diLeu motif binding sites on AP2. Only a minimal conformation change from the closed state is absolutely required to expose the diLeu binding site, and in this partially unlocked conformation, the canonical Yxxφ binding site remains inaccessible (Canagarajah et al., 2013). Full activation is necessary to accommodate Yxxφ motif, and this might be accompanied by efficient release of auto-inhibitory binding between the β2 and μ2 subunits to fully expose the clathrin binding site (Kelly et al., 2008; Jackson et al., 2010). Hence, unlike diLeu motif binding to AP2, the global disruption of interaction of Yxxφ with AP2 has profound consequences on CCP nucleation. Based on our observations and existing structural evidence, we can conclude that a broad spectrum of attainable AP2 conformations can drive cargo sorting. It still needs to be determined whether and how this differential regulation affects sorting of the 858 receptors identified in our screen containing both types of the motifs.

Interestingly, both diLeu and Yxxφ motifs are subject to regulation by phosphorylation. For example, phosphorylation of Ser residues in the vicinity of diLeu motifs is known to enhance their interaction with AP2 (Pitcher et al., 1999). In contrast, tyrosine phosphorylation within Yxxφ motifs negatively regulates their interaction with AP2 (Marchese et al., 2008; Traub and Bonifacino, 2013). Most likely, various posttranslational modifications in cargo, as well as adaptors, act together with internalization motifs to regulate cargo sorting into CCPs. Therefore future experiments will unravel the temporal and functional hierarchy of kinase and phosphatase networks in signaling cascades that orchestrate cargo sensing during CCP formation.

AP2 is indispensable for normal embryonic development and CME in vertebrates, *Drosophila melanogaster*, and

Caenorhabditis elegans (González-Gaitán and Jäckle, 1997; Mitsunari et al., 2005; Gu et al., 2008); however, it is not required for viability or CME in yeast (Weinberg and Drubin, 2012). In yeast, the initiation phase of CME is remarkably flexible, such that many early-arriving adaptors, including homologues for Eps15 and FCHo, share the initiation function in a potentially redundant manner (Brach et al., 2014). Unlike in mammalian cells, monoubiquitylation is the main internalization signal, and all of the yeast initiation components contain ubiquitin-binding domains (Weinberg and Drubin, 2012). Strikingly, neither PIP2 (Sun and Drubin, 2012) nor Yxxφ interactions are required for nucleation of endocytic sites in yeast. There are fewer endocytic Yxxφ-containing cargoes (Munn, 2001; Weinberg and Drubin, 2012), and the critical residue in the Yxxφ-binding site on μ2 is not conserved in yeast. Thus, AP2 complexes appear to have evolved their role in mammals as allosteric regulators of CCP nucleation, through PIP2 and cargo interactions. We propose that this functional hierarchy, based on allosteric regulation of AP2 activity, provides a mechanism to link cargo capture and sorting with CCP initiation and to provide greater spatial and temporal control of CME in mammalian cells.

Materials and methods

Generation of constructs and viruses

AP2 μ and α constructs. The AP2 μ2 and α sequences were generated using standard site-directed mutagenesis within siRNA-resistant cDNA encoding the full-length subunits, provided by M.S. Robinson (Cambridge Institute for Medical Research, Cambridge, England, UK; Motley et al., 2006). The α subunit contained a brain-specific splice insert, whereas the μ2 subunit contained a myc tag within flexible linkers (Motley et al., 2006). Resulting cDNAs were inserted into retroviral bicistronic IRES vector PMIB6 (Aguet et al., 2013) using conventional restriction enzyme cloning techniques.

AP2 β construct. cDNA encoding human isoform 1 of the full-length AP2β subunit (937 aa; Uniprot identifier P63010-1) was obtained from C. Antonescu (Ryerson University, Toronto, ON, Canada). An siRNA-resistant form was created by silent mutation of the siRNA target sequence 5′-TGGCAGAACTGAAAGAATA-3′ to 5′-TGGCAGAGTTAAAAGAATA-3′ (underline denotes changes). For the recognition of ectopically expressed AP2β, a Flag tag sequence (DYKDDDDK) was inserted by PCR into the cDNA at residue 602 within the flexible linker region. The $\beta2^{PIP2-}$ plasmid was generated by inserting a mutant fragment containing residues 5E/12E/26E/27E/29E/36E acquired as "gblock" (Integrated DNA Technologies) using conventional cloning techniques with restriction enzymes.

AP2 σ construct. cDNA encoding AP2σ with a C-terminal Flag-tag was acquired as a gBlock DNA fragment (Integrated DNA Technologies), designed as a Megaprimer (Miyazaki, 2011) that contained flanking 24-bp-long regions of homology to PMIB6 for its insertion by PCR. Four silent mutations conferring siRNA resistance were designed in the siRNA target sequence 5′-CTTCGTGGAGGTCTTAAACGA-3′ to 5′-TTTTGTAGAAGTCTTAAACGA-3′. The σ2 sequence was altered by point mutation V88D to abrogate the diLeu-motif binding using standard site-directed mutagenesis.

CD8 chimeras. cDNAs coding for CD8-YAAL or CD8-EAAALL chimeras were provided by M.S. Robinson (Kozik et al., 2010). cDNAs were subcloned from the original PiresNeo2 vector into an adenoviral pADTET T3T7 vector by seamless cloning and in vivo recombination (Lu, 2005).

Preparation of viruses. Recombinant adenoviruses for tet-regulated CD8 chimeras were generated as previously described (Hardy et al., 1997; Damke et al., 2001). Retroviruses encoding AP2 adaptins were generated as previously described (Aguet et al., 2013).

Cell culture

htertRPE-1 cells were obtained from ATCC and used because they have a normal karyotype, are suitable for genome editing, are nontransformed, and have a diffraction-limited and dynamic population of CCPs when seeded on gelatin. htertRPE-1 cells stably expressing CLCa-EGFP and reconstituted with WT or mutant AP2 subunits were derived as previously described (Aguet et al., 2013). In brief, CLCa-EGFP–expressing cells were infected with retrovirus and FACS-sorted 3 d after infection into cohorts based on BFP fluorescence. Stable cell lines expressing near-endogenous levels of α, β2, μ2, and σ2 adaptins as determined by Western blotting using the anti-α (#AC1-M11; Thermo Fisher Scientific), anti-μ2 polyclonal antibody R11-29 (gift of J. Bonifacino, National Institutes of Health, Bethesda, MD; Aguilar et al., 1997), anti-AP2σ mAb ab128950 (Abcam), anti-AP2β ab75158 (Abcam), mAb anti–Flag tag M1 (Sigma-Aldrich), and anti–Myc tag antibody clone 9E10 (EMD Millipore) were chosen for further experiments. All cell lines were grown under 5% CO_2 at 37°C in DMEM high-glucose medium (Thermo Fisher Scientific) supplemented with 10% (vol/vol) FCS (HyClone).

siRNA transfection

Cells grown in 6-cm dishes were treated with siRNA sequences to silence the endogenous AP2 subunit. 170 pmol of siRNA was mixed with RNAiMAX reagent in 0.5 ml of OptiMEM (Thermo Fisher Scientific). The mixture was incubated at RT for 20 min, added to cells, and incubated with cells for 4 h. Transfection was performed 12, 36, and 60 h after plating, and experiments were performed on the fifth day. The control "AllStars negative" siRNA nontargeting sequence was purchased from QIAGEN.

Transferrin receptor internalization

TfnR internalization was assessed using a modified protocol described by (Reis et al., 2015). Mouse anti-TfnR mAb (HTR-D65, generated in-house from hybridomas; Schmid and Smythe, 1991) at a concentration of 4 μg/ml was added to the cells at 37°C at time 0 of internalization. After 5 min at 37°C, during the linear phase of uptake, cells were transferred to 4°C to stop internalization. To assess TfnR internalization upon AAK1 inhibition, cells were preincubated for 3 h at 37°C with 10 μM Compound 2 (a previously published AAK1 inhibitor [Bamborough et al., 2008]) or the equivalent final concentration of DMSO (0.1% vol/vol) as a control. For uptake experiments, the anti-TfnR mAb solution was made in medium containing the same concentration of DMSO or inhibitor.

CD8 chimera internalization and immunofluorescence

Cells were coinfected in suspension with adenoviruses encoding the CD8 chimeras and adenoviruses encoding a tet repressible transcription activator. In brief, cells were detached by trypsinization, washed once with DMEM, and resuspended in 4 ml of DMEM containing both types of adenovirus and tetracycline at a concentration of 15 ng/ml. Cells were seeded either on gelatin-coated coverslips (for immunofluorescence) or into 96-well plates at a density of 3×10^4 cells per well (for internalization assays). Localization or internalization of CD8 chimera was followed by anti-CD8 mAb UCHT-4 (C7423; Sigma-Aldrich) 12–16 h after infection.

TIRF microscopy and quantification

TIRF microscopy was performed as previously described (Loerke et al., 2009). Cells were imaged on gelatin-coated coverslips 5–12 h after

seeding. In brief, cells expressing EGFP-CLCa and AP2 subunits were imaged using a 100×, 1.49-NA Apo TIRF objective (Nikon) mounted on a Ti-Eclipse inverted microscope equipped with the Perfect Focus System (Nikon). Time-lapse image sequences from different cells were acquired at a frame rate of 1 frame/s and exposure time of 150 ms using a CoolSNAP HQ2 monochrome CCD camera with 6.45 × 6.45 μm^2 pixels (Photometrics). Similarly, nearly simultaneous two-channel (e.g., 488-nm epifluorescence/TIRF or 488/561-nm TIRF) movies were acquired at 0.5 frame/s with exposure times of 200 ms (EGFP-CLCa; for epifluorescence excitation), and 200–300 ms (overexpressed Dnm2-mRuby2; for TIRF excitation). Quantitative analysis to distinguish bona fide CCPs from all detected CLSs, and to measure CCP initiation rates and lifetime distributions, was performed exactly as previously described (Aguet et al., 2013).

The quantitative analysis of CCPs and sCLSs was previously described and developed (Aguet et al., 2013). In brief, our analysis focuses on diffraction-limited objects; therefore, the detection of all CLSs is based on the assumption that the fluorescent signals measured can be described by a Gaussian point spread function. Signals were selected as valid CLS detections if the amplitude was higher than a 95th percentile confidence threshold in the local background noise distribution. CLS trajectories were calculated from the detections obtained in individual frames using the u-track software package (Jaqaman et al., 2008). Bona fide CCPs that undergo stabilization and maturation are distinguished from transient sCLCs based on quantitative analysis of the progression of their CLCa-EGFP fluorescence intensity during early stages of growth, as previously described (Aguet et al., 2013). CCP initiation rates were calculated as the number of bona fide CCPs per surface area and unit time. Initiation rates of sCLCs were determined by subtracting the rate of bona fide CCP initiation from the rate of initiation of all detected CLSs.

Calculation of clathrin recruitment rates

Clathrin recruitment rates were determined using the approach outlined in Loerke et al. (2011): all available CCP trajectories of a given total lifetime τ were averaged and smoothed with a box filter to produce a single lifetime bin, i.e., the representative intensity time course $I(t,\tau)$, with t being the elapsed time. The clathrin recruitment rate for each total lifetime τ was the slope of the intensity time course $I(t,\tau)$ averaged in the time interval t = 3–8 s after the CCP's first visible (i.e., detected) time point. Raw recruitment rates were calculated in units of intensity counts per second. For all conditions, the measured recruitment rates increased with total CCP lifetime τ and typically stabilized at approximately τ = 45 s.

Immunofluorescence microscopy

Cells seeded on gelatin-coated coverslips were fixed and permeabilized according to previously published protocols (Mettlen et al., 2010). AP2 was detected using mouse anti-AP2 mAb (AP6, generated in-house from hybridomas; Chin et al., 1989). Transmembrane proteins were detected using mouse anti–EGF receptor mAb AB11 (199.12; NeoMarkers), mAb anti-TfnR HTR-D65, and mouse anti-CD8 mAb (UCHT-4, C7423; Sigma-Aldrich). Fixed cell images were acquired by TIRF microscopy.

Quantification of colocalization

Quantitative colocalization analysis was used to compare the stoichiometry of AP2 with respect to CLCa-EGFP in CCPs of mutant and control cells. The Pearson correlation coefficient was calculated using image analysis software Imaris 7.4 and ImarisColoc according to established protocols (Pompey et al., 2013). In brief, images were preprocessed to exclude background fluorescence in the green channel so as to analyze only CCPs. Next, intensity thresholds were automatically established for both channels using a point spread function value of 0.3 µm. The Pearson correlation coefficient for CCPs was calculated for five images containing up to three cells, and values for 20 images were pooled for statistical analysis.

Computational screen for short endocytic motifs

We performed a computational screen to determine the relative abundance of diLeu- and Yxxφ-based motifs across cytosolic domains of human transmembrane proteins that annotate as being localized to the plasma membrane. The amino acid composition of the short motifs included in the screen were as follows. For Yxxφ-based motifs, we allowed φ = L, I, M, F, or V. For diLeu motifs, we used the following search X[D/E]XXXL[L/I]; for phosphorylation-dependent diLeu motifs, [S/T*]XXXXL[L/I]; and for noncanonical diLeu motifs, X[R/H/Q] XXXL[L/I] to ensure capture of their greater heterogeneity (Traub and Bonifacino, 2013). We queried the UnitProt database for all proteins matching the following search term: annotation:(type:topo_dom cytoplasmic) annotation:(type:transmem) AND reviewed:yes AND organism":Homo sapiens (Human) [9606]." This query returned 3,730 sequences, from which duplicate records were removed, yielding a total of 3,705 proteins. We then searched the cytosolic domains of each sequence, using UniProt's domain range annotations, for the presence of either diLeu motifs or Yxxφ-based motifs. We identified a total of 2,383 proteins with at least one motif, and we compared the presence of tyrosine and diLeu motifs across these proteins. Overall, tyrosine motifs were approximately five times more prevalent. All computational analyses were conducted using custom Python and R scripts, which are included in the supplemental material.

Online supplemental material

Fig. S1 shows Western blots of AP2 complex immunoprecipitations and immunofluorescence images that validate the mutants studied. Fig. S2 shows fluorescence analyses of clathrin assembly during CCP maturation in α^{WT} and α^{PIP2-} cells. Fig. S3 shows Pearson correlation coefficient data for localization of cargo and AP2 complexes with CCPs in α^{WT} and α^{PIP2-} cells. Fig. S4 shows internalization efficiency of TfnRs and epifluorescence/TIRF data for CCPs in $\mu2^{WT}$ and $\mu2^{PIP2-}$ cells, as well as Western blots showing levels of phosphorylation of µ2 at T156 under various conditions. Fig. S5 shows immunofluorescence and Western blots validating expression levels of model Y–based and diLeu-based cargo receptors in htertRPE cells.

Acknowledgments

We thank Philippe Roudot and Gaudenz Danuser for help with quantification of our data. We are grateful to Wesley Burford for adenovirus production, Margaret S. Robinson for CD8 and AP2 constructs, David J. Owen for helpful discussions and insights, and W. Mike Henne for comments that greatly improved the manuscript. We thank Peter Michaely, Assaf Zaritsky, and all members of the Schmid laboratory for helpful discussions.

This research was supported by the People Program (Marie Curie Actions) of the European Union's Seventh Framework Programme grant agreement no. PIOF-GA-2012-330268, the Swiss National Science Foundation Fellowship for Prospective Researchers (to Z. Kadlecova), and National Institutes of Health grants MH61345 and GM73165 to S.L. Schmid.

The authors declare no competing financial interests.

Submitted: 21 August 2016
Revised: 31 October 2016
Accepted: 30 November 2016

References

Aguet, F., C.N. Antonescu, M. Mettlen, S.L. Schmid, and G. Danuser. 2013. Advances in analysis of low signal-to-noise images link dynamin and AP2 to the functions of an endocytic checkpoint. *Dev. Cell.* 26:279–291. http://dx.doi.org/10.1016/j.devcel.2013.06.019

Aguilar, R.C., H. Ohno, K.W. Roche, and J.S. Bonifacino. 1997. Functional domain mapping of the clathrin-associated adaptor medium chains μ1 and μ2. *J. Biol. Chem.* 272:27160–27166. http://dx.doi.org/10.1074/jbc.272.43.27160

Antonescu, C.N., F. Aguet, G. Danuser, and S.L. Schmid. 2011. Phosphatidylinositol-(4,5)-bisphosphate regulates clathrin-coated pit initiation, stabilization, and size. *Mol. Biol. Cell*. 22:2588–2600. http://dx.doi.org/10.1091/mbc.E11-04-0362

Bamborough, P., D. Drewry, G. Harper, G.K. Smith, and K. Schneider. 2008. Assessment of chemical coverage of kinome space and its implications for kinase drug discovery. *J. Med. Chem.* 51:7898–7914. http://dx.doi.org/10.1021/jm8011036

Boucrot, E., S. Saffarian, R. Massol, T. Kirchhausen, and M. Ehrlich. 2006. Role of lipids and actin in the formation of clathrin-coated pits. *Exp. Cell Res.* 312:4036–4048. http://dx.doi.org/10.1016/j.yexcr.2006.09.025

Brach, T., C. Godlee, I. Moeller-Hansen, D. Boeke, and M. Kaksonen. 2014. The initiation of clathrin-mediated endocytosis is mechanistically highly flexible. *Curr. Biol.* 24:548–554. http://dx.doi.org/10.1016/j.cub.2014.01.048

Canagarajah, B.J., X. Ren, J.S. Bonifacino, and J.H. Hurley. 2013. The clathrin adaptor complexes as a paradigm for membrane-associated allostery. *Protein Sci.* 22:517–529. http://dx.doi.org/10.1002/pro.2235

Chin, D.J., R.M. Straubinger, S. Acton, I. Näthke, and F.M. Brodsky. 1989. 100-kDa polypeptides in peripheral clathrin-coated vesicles are required for receptor-mediated endocytosis. *Proc. Natl. Acad. Sci. USA*. 86:9289–9293. http://dx.doi.org/10.1073/pnas.86.23.9289

Cocucci, E., F. Aguet, S. Boulant, and T. Kirchhausen. 2012. The first five seconds in the life of a clathrin-coated pit. *Cell.* 150:495–507. http://dx.doi.org/10.1016/j.cell.2012.05.047

Collins, B.M., A.J. McCoy, H.M. Kent, P.R. Evans, and D.J. Owen. 2002. Molecular architecture and functional model of the endocytic AP2 complex. *Cell.* 109:523–535. http://dx.doi.org/10.1016/S0092-8674(02)00735-3

Conner, S.D., and S.L. Schmid. 2002. Identification of an adaptor-associated kinase, AAK1, as a regulator of clathrin-mediated endocytosis. *J. Cell Biol.* 156:921–929. http://dx.doi.org/10.1083/jcb.200108123

Conner, S.D., and S.L. Schmid. 2003. Regulated portals of entry into the cell. *Nature.* 422:37–44. http://dx.doi.org/10.1038/nature01451

Conner, S.D., T. Schröter, and S.L. Schmid. 2003. AAK1-mediated micro2 phosphorylation is stimulated by assembled clathrin. *Traffic.* 4:885–890. http://dx.doi.org/10.1046/j.1398-9219.2003.0142.x

Damke, H., D.D. Binns, H. Ueda, S.L. Schmid, and T. Baba. 2001. Dynamin GTPase domain mutants block endocytic vesicle formation at morphologically distinct stages. *Mol. Biol. Cell.* 12:2578–2589. http://dx.doi.org/10.1091/mbc.12.9.2578

Dannhauser, P.N., and E.J. Ungewickell. 2012. Reconstitution of clathrin-coated bud and vesicle formation with minimal components. *Nat. Cell Biol.* 14:634–639. http://dx.doi.org/10.1038/ncb2478

Ehrlich, M., W. Boll, A. Van Oijen, R. Hariharan, K. Chandran, M.L. Nibert, and T. Kirchhausen. 2004. Endocytosis by random initiation and stabilization of clathrin-coated pits. *Cell.* 118:591–605. http://dx.doi.org/10.1016/j.cell.2004.08.017

Ferguson, S.M., and P. De Camilli. 2012. Dynamin, a membrane-remodelling GTPase. *Nat. Rev. Mol. Cell Biol.* 13:75–88. http://dx.doi.org/10.1038/nrm3266

Gaidarov, I., and J.H. Keen. 1999. Phosphoinositide-AP-2 interactions required for targeting to plasma membrane clathrin-coated pits. *J. Cell Biol.* 146:755–764. http://dx.doi.org/10.1083/jcb.146.4.755

Gaidarov, I., F. Santini, R.A. Warren, and J.H. Keen. 1999. Spatial control of coated-pit dynamics in living cells. *Nat. Cell Biol.* 1:1–7.

Godlee, C., and M. Kaksonen. 2013. From uncertain beginnings: Initiation mechanisms of clathrin-mediated endocytosis. *J. Cell Biol.* 203:717–725. http://dx.doi.org/10.1083/jcb.201307100

González-Gaitán, M., and H. Jäckle. 1997. Role of *Drosophila* alpha-adaptin in presynaptic vesicle recycling. *Cell.* 88:767–776. http://dx.doi.org/10.1016/S0092-8674(00)81923-6

Grassart, A., A.T. Cheng, S.H. Hong, F. Zhang, N. Zenzer, Y. Feng, D.M. Briner, G.D. Davis, D. Malkov, and D.G. Drubin. 2014. Actin and dynamin2 dynamics and interplay during clathrin-mediated endocytosis. *J. Cell Biol.* 205:721–735. http://dx.doi.org/10.1083/jcb.201403041

Gu, M., K. Schuske, S. Watanabe, Q. Liu, P. Baum, G. Garriga, and E.M. Jorgensen. 2008. Mu2 adaptin facilitates but is not essential for synaptic vesicle recycling in *Caenorhabditis elegans*. *J. Cell Biol.* 183:881–892. http://dx.doi.org/10.1083/jcb.200806088

Hardy, S., M. Kitamura, T. Harris-Stansil, Y. Dai, and M.L. Phipps. 1997. Construction of adenovirus vectors through Cre-lox recombination. *J. Virol.* 71:1842–1849.

Hollopeter, G., J.J. Lange, Y. Zhang, T.N. Vu, M. Gu, M. Ailion, E.J. Lambie, B.D. Slaughter, J.R. Unruh, L. Florens, and E.M. Jorgensen. 2014. The membrane-associated proteins FCHo and SGIP are allosteric activators of the AP2 clathrin adaptor complex. *eLife*. 3:. http://dx.doi.org/10.7554/eLife.03648

Höning, S., D. Ricotta, M. Krauss, K. Späte, B. Spolaore, A. Motley, M. Robinson, C. Robinson, V. Haucke, and D.J. Owen. 2005. Phosphatidylinositol-(4,5)-bisphosphate regulates sorting signal recognition by the clathrin-associated adaptor complex AP2. *Mol. Cell.* 18:519–531. http://dx.doi.org/10.1016/j.molcel.2005.04.019

Jackson, A.P., A. Flett, C. Smythe, L. Hufton, F.R. Wettey, and E. Smythe. 2003. Clathrin promotes incorporation of cargo into coated pits by activation of the AP2 adaptor micro2 kinase. *J. Cell Biol.* 163:231–236. http://dx.doi.org/10.1083/jcb.200304079

Jackson, L.P., B.T. Kelly, A.J. McCoy, T. Gaffry, L.C. James, B.M. Collins, S. Höning, P.R. Evans, and D.J. Owen. 2010. A large-scale conformational change couples membrane recruitment to cargo binding in the AP2 clathrin adaptor complex. *Cell.* 141:1220–1229. http://dx.doi.org/10.1016/j.cell.2010.05.006

Jaqaman, K., D. Loerke, M. Mettlen, H. Kuwata, S. Grinstein, S.L. Schmid, and G. Danuser. 2008. Robust single-particle tracking in live-cell time-lapse sequences. *Nat. Methods*. 5:695–702. http://dx.doi.org/10.1038/nmeth.1237

Kelly, B.T., A.J. McCoy, K. Späte, S.E. Miller, P.R. Evans, S. Höning, and D.J. Owen. 2008. A structural explanation for the binding of endocytic dileucine motifs by the AP2 complex. *Nature.* 456:976–979. http://dx.doi.org/10.1038/nature07422

Kelly, B.T., S.C. Graham, N. Liska, P.N. Dannhauser, S. Höning, E.J. Ungewickell, and D.J. Owen. 2014. Clathrin adaptors. AP2 controls clathrin polymerization with a membrane-activated switch. *Science.* 345:459–463. http://dx.doi.org/10.1126/science.1254836

Kirchhausen, T., D. Owen, and S.C. Harrison. 2014. Molecular structure, function, and dynamics of clathrin-mediated membrane traffic. *Cold Spring Harb. Perspect. Biol.* 6:a016725. http://dx.doi.org/10.1101/cshperspect.a016725

Kozik, P., R.W. Francis, M.N. Seaman, and M.S. Robinson. 2010. A screen for endocytic motifs. *Traffic.* 11:843–855. http://dx.doi.org/10.1111/j.1600-0854.2010.01056.x

Liu, A.P., F. Aguet, G. Danuser, and S.L. Schmid. 2010. Local clustering of transferrin receptors promotes clathrin-coated pit initiation. *J. Cell Biol.* 191:1381–1393. http://dx.doi.org/10.1083/jcb.201008117

Loerke, D., M. Mettlen, D. Yarar, K. Jaqaman, H. Jaqaman, G. Danuser, and S.L. Schmid. 2009. Cargo and dynamin regulate clathrin-coated pit maturation. *PLoS Biol.* 7:e57. http://dx.doi.org/10.1371/journal.pbio.1000057

Loerke, D., M. Mettlen, S.L. Schmid, and G. Danuser. 2011. Measuring the hierarchy of molecular events during clathrin-mediated endocytosis. *Traffic.* 12:815–825. http://dx.doi.org/10.1111/j.1600-0854.2011.01197.x

Lu, Q. 2005. Seamless cloning and gene fusion. *Trends Biotechnol.* 23:199–207. http://dx.doi.org/10.1016/j.tibtech.2005.02.008

Ma, L., P.K. Umasankar, A.G. Wrobel, A. Lymar, A.J. McCoy, S.S. Holkar, A. Jha, T. Pradhan-Sundd, S.C. Watkins, D.J. Owen, and L.M. Traub. 2016. Transient Fcho1/2·Eps15/R·AP-2 nanoclusters prime the AP-2 clathrin adaptor for cargo binding. *Dev. Cell*. 37:428–443. http://dx.doi.org/10.1016/j.devcel.2016.05.003

Marchese, A., M.M. Paing, B.R. Temple, and J. Trejo. 2008. G protein-coupled receptor sorting to endosomes and lysosomes. *Annu. Rev. Pharmacol. Toxicol.* 48:601–629. http://dx.doi.org/10.1146/annurev.pharmtox.48.113006.094646

Mattera, R., M. Boehm, R. Chaudhuri, Y. Prabhu, and J.S. Bonifacino. 2011. Conservation and diversification of dileucine signal recognition by adaptor protein (AP) complex variants. *J. Biol. Chem.* 286:2022–2030. http://dx.doi.org/10.1074/jbc.M110.197178

McMahon, H.T., and E. Boucrot. 2011. Molecular mechanism and physiological functions of clathrin-mediated endocytosis. *Nat. Rev. Mol. Cell Biol.* 12:517–533. http://dx.doi.org/10.1038/nrm3151

Merrifield, C.J., and M. Kaksonen. 2014. Endocytic accessory factors and regulation of clathrin-mediated endocytosis. *Cold Spring Harb. Perspect. Biol.* 6:a016733. http://dx.doi.org/10.1101/cshperspect.a016733

Merrifield, C.J., M.E. Feldman, L. Wan, and W. Almers. 2002. Imaging actin and dynamin recruitment during invagination of single clathrin-coated pits. *Nat. Cell Biol.* 4:691–698. http://dx.doi.org/10.1038/ncb837

Mettlen, M., and G. Danuser. 2014. Imaging and modeling the dynamics of clathrin-mediated endocytosis. *Cold Spring Harb. Perspect. Biol.* 6:a017038. http://dx.doi.org/10.1101/cshperspect.a017038

Mettlen, M., D. Loerke, D. Yarar, G. Danuser, and S.L. Schmid. 2010. Cargo- and adaptor-specific mechanisms regulate clathrin-mediated endocytosis. *J. Cell Biol.* 188:919–933. http://dx.doi.org/10.1083/jcb.200908078

Mitsunari, T., F. Nakatsu, N. Shioda, P.E. Love, A. Grinberg, J.S. Bonifacino, and H. Ohno. 2005. Clathrin adaptor AP-2 is essential for early embryonal development. *Mol. Cell. Biol.* 25:9318–9323. http://dx.doi.org/10.1128/MCB.25.21.9318-9323.2005

Miyazaki, K. 2011. MEGAWHOP cloning: A method of creating random mutagenesis libraries via megaprimer PCR of whole plasmids. *Methods Enzymol.* 498:399–406. http://dx.doi.org/10.1016/B978-0-12-385120-8.00017-6

Morlot, S., and A. Roux. 2013. Mechanics of dynamin-mediated membrane fission. *Annu. Rev. Biophys.* 42:629–649. http://dx.doi.org/10.1146/annurev-biophys-050511-102247

Motley, A.M., N. Berg, M.J. Taylor, D.A. Sahlender, J. Hirst, D.J. Owen, and M.S. Robinson. 2006. Functional analysis of AP-2 α and μ2 subunits. *Mol. Biol. Cell.* 17:5298–5308. http://dx.doi.org/10.1091/mbc.E06-05-0452

Munn, A.L. 2001. Molecular requirements for the internalisation step of endocytosis: Insights from yeast. *Biochim. Biophys. Acta.* 1535:236–257. http://dx.doi.org/10.1016/S0925-4439(01)00028-X

Ohno, H., J. Stewart, M.C. Fournier, H. Bosshart, I. Rhee, S. Miyatake, T. Saito, A. Gallusser, T. Kirchhausen, and J.S. Bonifacino. 1995. Interaction of tyrosine-based sorting signals with clathrin-associated proteins. *Science.* 269:1872–1875. http://dx.doi.org/10.1126/science.7569928

Ohno, H., M.C. Fournier, G. Poy, and J.S. Bonifacino. 1996. Structural determinants of interaction of tyrosine-based sorting signals with the adaptor medium chains. *J. Biol. Chem.* 271:29009–29015. http://dx.doi.org/10.1074/jbc.271.46.29009

Olusanya, O., P.D. Andrews, J.R. Swedlow, and E. Smythe. 2001. Phosphorylation of threonine 156 of the mu2 subunit of the AP2 complex is essential for endocytosis in vitro and in vivo. *Curr. Biol.* 11:896–900. http://dx.doi.org/10.1016/S0960-9822(01)00240-8

Owen, D.J., and P.R. Evans. 1998. A structural explanation for the recognition of tyrosine-based endocytotic signals. *Science.* 282:1327–1332. http://dx.doi.org/10.1126/science.282.5392.1327

Owen, D.J., Y. Vallis, M.E. Noble, J.B. Hunter, T.R. Dafforn, P.R. Evans, and H.T. McMahon. 1999. A structural explanation for the binding of multiple ligands by the alpha-adaptin appendage domain. *Cell.* 97:805–815. http://dx.doi.org/10.1016/S0092-8674(00)80791-6

Owen, D.J., B.M. Collins, and P.R. Evans. 2004. Adaptors for clathrin coats: Structure and function. *Annu. Rev. Cell Dev. Biol.* 20:153–191. http://dx.doi.org/10.1146/annurev.cellbio.20.010403.104543

Pandey, K.N. 2009. Functional roles of short sequence motifs in the endocytosis of membrane receptors. *Front. Biosci. (Landmark Ed.).* 14:5339–5360. http://dx.doi.org/10.2741/3599

Pelkmans, L., E. Fava, H. Grabner, M. Hannus, B. Habermann, E. Krausz, and M. Zerial. 2005. Genome-wide analysis of human kinases in clathrin- and caveolae/raft-mediated endocytosis. *Nature.* 436:78–86. http://dx.doi.org/10.1038/nature03571

Perkins, J.R., I. Diboun, B.H. Dessailly, J.G. Lees, and C. Orengo. 2010. Transient protein-protein interactions: structural, functional, and network properties. *Structure.* 18:1233–1243. http://dx.doi.org/10.1016/j.str.2010.08.007

Pitcher, C., S. Höning, A. Fingerhut, K. Bowers, and M. Marsh. 1999. Cluster of differentiation antigen 4 (CD4) endocytosis and adaptor complex binding require activation of the CD4 endocytosis signal by serine phosphorylation. *Mol. Biol. Cell.* 10:677–691. http://dx.doi.org/10.1091/mbc.10.3.677

Pompey, S.N., P. Michaely, and K. Luby-Phelps. 2013. Quantitative fluorescence co-localization to study protein-receptor complexes. *Methods Mol. Biol.* 1008:439–453. http://dx.doi.org/10.1007/978-1-62703-398-5_16

Praefcke, G.J., M.G. Ford, E.M. Schmid, L.E. Olesen, J.L. Gallop, S.Y. Peak-Chew, Y. Vallis, M.M. Babu, I.G. Mills, and H.T. McMahon. 2004. Evolving nature of the AP2 alpha-appendage hub during clathrin-coated vesicle endocytosis. *EMBO J.* 23:4371–4383. http://dx.doi.org/10.1038/sj.emboj.7600445

Reis, C.R., P.H. Chen, S. Srinivasan, F. Aguet, M. Mettlen, and S.L. Schmid. 2015. Crosstalk between Akt/GSK3β signaling and dynamin-1 regulates clathrin-mediated endocytosis. *EMBO J.* 34:2132–2146. http://dx.doi.org/10.15252/embj.201591518

Ricotta, D., S.D. Conner, S.L. Schmid, K. von Figura, and S. Honing. 2002. Phosphorylation of the AP2 mu subunit by AAK1 mediates high affinity binding to membrane protein sorting signals. *J. Cell Biol.* 156:791–795. http://dx.doi.org/10.1083/jcb.200111068

Rohde, G., D. Wenzel, and V. Haucke. 2002. A phosphatidylinositol (4,5)-bisphosphate binding site within mu2-adaptin regulates clathrin-mediated endocytosis. *J. Cell Biol.* 158:209–214. http://dx.doi.org/10.1083/jcb.200203103

Saffarian, S., and T. Kirchhausen. 2008. Differential evanescence nanometry: Live-cell fluorescence measurements with 10-nm axial resolution on the plasma membrane. *Biophys. J.* 94:2333–2342. http://dx.doi.org/10.1529/biophysj.107.117234

Schledzewski, K., H. Brinkmann, and R.R. Mendel. 1999. Phylogenetic analysis of components of the eukaryotic vesicle transport system reveals a common origin of adaptor protein complexes 1, 2, and 3 and the F subcomplex of the coatomer COPI. *J. Mol. Evol.* 48:770–778. http://dx.doi.org/10.1007/PL00006521

Schmid, E.M., and H.T. McMahon. 2007. Integrating molecular and network biology to decode endocytosis. *Nature.* 448:883–888. http://dx.doi.org/10.1038/nature06031

Schmid, S.L., and V.A. Frolov. 2011. Dynamin: functional design of a membrane fission catalyst. *Annu. Rev. Cell Dev. Biol.* 27:79–105. http://dx.doi.org/10.1146/annurev-cellbio-100109-104016

Schmid, S.L., and E. Smythe. 1991. Stage-specific assays for coated pit formation and coated vesicle budding in vitro. *J. Cell Biol.* 114:869–880. http://dx.doi.org/10.1083/jcb.114.5.869

Shih, W., A. Gallusser, and T. Kirchhausen. 1995. A clathrin-binding site in the hinge of the β2 chain of mammalian AP-2 complexes. *J. Biol. Chem.* 270:31083–31090. http://dx.doi.org/10.1074/jbc.270.52.31083

Sun, Y., and D.G. Drubin. 2012. The functions of anionic phospholipids during clathrin-mediated endocytosis site initiation and vesicle formation. *J. Cell Sci.* 125:6157–6165. http://dx.doi.org/10.1242/jcs.115741

Taylor, M.J., D. Perrais, and C.J. Merrifield. 2011. A high precision survey of the molecular dynamics of mammalian clathrin-mediated endocytosis. *PLoS Biol.* 9:e1000604. http://dx.doi.org/10.1371/journal.pbio.1000604

Taylor, M.J., M. Lampe, and C.J. Merrifield. 2012. A feedback loop between dynamin and actin recruitment during clathrin-mediated endocytosis. *PLoS Biol.* 10:e1001302. http://dx.doi.org/10.1371/journal.pbio.1001302

Traub, L.M. 2009. Tickets to ride: Selecting cargo for clathrin-regulated internalization. *Nat. Rev. Mol. Cell Biol.* 10:583–596. http://dx.doi.org/10.1038/nrm2751

Traub, L.M., and J.S. Bonifacino. 2013. Cargo recognition in clathrin-mediated endocytosis. *Cold Spring Harb. Perspect. Biol.* 5:a016790. http://dx.doi.org/10.1101/cshperspect.a016790

Traub, L.M., M.A. Downs, J.L. Westrich, and D.H. Fremont. 1999. Crystal structure of the alpha appendage of AP-2 reveals a recruitment platform for clathrin-coat assembly. *Proc. Natl. Acad. Sci. USA.* 96:8907–8912. http://dx.doi.org/10.1073/pnas.96.16.8907

Umasankar, P.K., L. Ma, J.R. Thieman, A. Jha, B. Doray, S.C. Watkins, and L.M. Traub. 2014. A clathrin coat assembly role for the muniscin protein central linker revealed by TALEN-mediated gene editing. *eLife*. 3:e04137. http://dx.doi.org/10.7554/eLife.04137

Van Roey, K., T.J. Gibson, and N.E. Davey. 2012. Motif switches: Decision-making in cell regulation. *Curr. Opin. Struct. Biol.* 22:378–385. http://dx.doi.org/10.1016/j.sbi.2012.03.004

Weinberg, J., and D.G. Drubin. 2012. Clathrin-mediated endocytosis in budding yeast. *Trends Cell Biol.* 22:1–13. http://dx.doi.org/10.1016/j.tcb.2011.09.001

Zoncu, R., R.M. Perera, R. Sebastian, F. Nakatsu, H. Chen, T. Balla, G. Ayala, D. Toomre, and P.V. De Camilli. 2007. Loss of endocytic clathrin-coated pits upon acute depletion of phosphatidylinositol 4,5-bisphosphate. *Proc. Natl. Acad. Sci. USA.* 104:3793–3798. http://dx.doi.org/10.1073/pnas.0611733104